JOURNAL OF PROPULSION AND POWER
Vol. 15, No. 1, January–February

Assessment of Parameters Influencing the Prediction of Shear-Layer Mixing

T. J. Barber* and L. M. Chiappetta†
United Technologies Research Center, East Hartford, Connecticut 06108
and
J. R. DeBonis,‡ N. J. Georgiadis,‡ and D. A. Yoder‡
NASA Lewis Research Center, Cleveland, Ohio 44135

A multisite team has completed an investigation of modeling high-speed mixing layers using the computational methods currently being applied to predict high-speed civil transport (HSCT) nozzle flowfields. The objectives of this investigation were to 1) calibrate the codes used by the various team members against the same benchmark experimental data, and 2) assess the accuracy of the Navier–Stokes codes in calculating turbulent flows having flow characteristics similar to those of HSCT engine nozzles by varying user-specified input parameters, e.g., grid, turbulence model, boundary conditions. Two flow geometries were investigated using the five codes of NASTAR, PAB3D, GIF3D, NASTD, and NPARC. The first was the heated supersonic round jet. For this configuration, with a jet-exit Mach number similar to that of the primary flow from mixer chutes, three nozzle flow temperatures were investigated with the five codes. Using the same grid, boundary conditions, and k-ϵ turbulence model (in the mixing region), very similar results were obtained for all codes, but the solutions did not agree well with the experimental velocity and temperature profiles. Further calculations using different turbulence models, compressibility corrections, and axisymmetric dissipation corrections improved the agreement with experimental data, but the corrections are not universally applicable. The second configuration was a two-dimensional supersonic mixing layer. For the flow case examined, with two supersonic streams, the five codes again produced very similar results using the same grid, boundary conditions, and turbulence model. The agreement with experimental data was better than for the round nozzle. Based on the results of this investigation, it was determined that consistent nozzle flow predictions may be obtained by the team members using the different codes investigated hereby using consistent computational grids, boundary conditions, and turbulence models. The deficiencies of these codes in predicting high-temperature compressible jets were identified and are directly related to the turbulence models currently employed. The consistency that was achieved will allow for a computational fluid dynamics procedure to be established for performing a multisite parametric design and analysis effort by the team members.

Nomenclature

a = speed of sound
D = nozzle exit plane diameter
k = turbulence kinetic energy
M = Mach number
P = pressure
T = temperature
U = axial velocity
X, R = axial, radial coordinates
X, Y = axial, vertical coordinates
ϵ = turbulence dissipation energy

Subscripts
a = ambient
c = convective
j = jet exit
t = total or stagnation

Presented as Paper 97-2639 at the AIAA/ASME/SAE/ASEE 33rd Joint Propulsion Conference, Seattle, WA, July 6–9, 1997; received Aug. 4, 1997; revision received June 24, 1998; accepted for publication July 6, 1998.

*Manager, Aeromechanical, Chemical and Fluid Systems Department. Associate Fellow AIAA.

†Senior Research Engineer, Aeromechanical, Chemical and Fluid Systems Department. Senior Member AIAA.

‡Aerospace Engineer, Turbomachinery and Propulsion Systems Division, Nozzle Branch. Member AIAA.

Introduction

THE classical approach for designing low-noise exhaust systems uses empirical rules and computational fluid dynamics (CFD) calculations aimed at lowering peak velocities and/or temperatures. Engineers need to be able to predict noise directly and use predictions to support their specific design goals. The computational approach typically used in most engineering organizations is some Navier–Stokes code applying state-of-the-art numerical procedures and physical models, e.g., turbulence, kinetics. In many current aerospace design efforts, multicompany teams, using different tools, contribute to the overall effort. The aim of the current study is to consider the viability of such a design process.

The pilot study under consideration is a mixer–ejector exhaust system under consideration for the high-speed civil transport (HSCT). In such a device, a supersonic hot primary flow exhausts into the ejector mixing duct. Cold external flow is simultaneously entrained into the duct and mixes with the primary flow. Viscous and shock-loss mechanisms drive the mixing process. The study will consider the dominant physical processes occurring within the mixer–ejector and will then identify what model problems best isolate these processes. These model problems will then be used to 1) calibrate the ability of the team member codes to produce consistent results, 2) assess the accuracy of the team member codes to predict mixing-dominated phenomena, and 3) identify the numerical and physical modeling issues that most strongly influence the prediction of mixing phenomena.

The key issues identified by representatives of the analysis team were compressibility; thermal effects; boundary conditions; turbulence modeling (constants, corrections, wall functions); geometrical influence on shear-layer development (planar vs round); streamwise vorticity; and numerics (code differences, grid, grid density ratio). This program addresses all of the high-priority items as well as some of the lower priority ones. To establish a common baseline for our studies, a set of common modeling rules were defined, using 1) common computational grid; 2) basic k-ε turbulence model (or its equivalent); 3) wall integration using low Reynolds number model; 4) common P_t, T_t upstream conditions; 5) turbulent Prandtl number, $Pr_t = 0.9$; and 6) upstream turbulence intensity $(k) = 1\%$.

In the following sections, relevant databases for code validation will be identified and candidate Navier–Stokes codes described. Subsequently, in the Results section, the codes will be first calibrated using the common or baseline input model and then these codes will be used to examine sensitivities to user-specified input data.

Validation Cases

Heated Supersonic Round Jet Without Coflow[1]

A water-cooled axisymmetric nozzle of diameter $D = 3.60$ in. (91.44 mm) was tested in the NASA Langley Research Center (LaRC) Jet Noise Laboratory. The nozzle design Mach number was 2.0 at $T_{tj} = 2000$°F. The nozzle operated at fully expanded conditions for the range of jet total temperatures considered in the test program. The flow Reynolds number, based D, varied from 2×10^6 to 3×10^6. Aerodynamic measurements of total temperature and pressure were obtained and provided by Seiner et al.[1] along the nozzle centerline using a water-cooled probe for a range of jet total temperatures (Table 1). Additional data, i.e., radial flow profiles and acoustic spectra, have not been provided. Over this range of temperatures, one can estimate the effects of compressibility in terms of the convective Mach number M_c, defined as

$$M_c = (U_j - U_\infty)/(a_j + a_\infty)$$

For the static ambient case under consideration, M_c varies from 0.87 to more than 1.25. These values correspond to a possible 60% reduction in shear-layer mixing rate, as measured by the so-called Langley curve.[2] Because the exit-flow Mach number of the nozzle used in the Seiner et al.[1] tests is similar to the exit-flow conditions from the mixer primary flow, this configuration is appropriate for 1) evaluating baseline performance of all candidate codes, 2) determining the effects of compressibility, and 3) determining the effects of large thermal gradients.

Planar Shear Layer[3–6]

This configuration considered two-stream, planar, turbulent, compressible mixing-layer experiments. Seven cases (1, 1d, 2, 3, 3r, 4, and 5) are available from the two-dimensional laser Doppler velocimetry (LDV) measurements of Refs. 3–6 (Table 2). These cases span a range of freestream velocity ratios, density ratios, and convective Mach numbers. The Reynolds number per unit length is 1×10^6 to 2×10^6. The experimenters recommend cases 2, 3, 4, and 5 as the most reliable for database purposes and CFD comparison. In all cases, the turbulent boundary-layer velocity profiles immediately upstream of the splitter plate tip were measured to establish the inflow boundary condition for the shear-layer flowfield.

Table 1 Seiner nozzle flow conditions

Run no.	T_{tj}, °F	T_{tj}, K	T_{tj}/T_a
6	104	313	1.00
21	455	508	1.62
31	515	541	1.73
41	900	755	2.41
51	1550	894	3.46
61	2000	1366	4.36

Table 2 Dutton and Goebel test conditions

Case	U_2/U	M_c	M_1	M_2	T_{t1}/T_{t2}
1	0.78	0.20	2.01	1.38	1.00
1d	0.79	0.20	2.02	1.39	1.00
2	0.57	0.46	1.91	1.36	1.96
3	0.18	0.69	1.96	0.27	1.00
3r	0.25	0.72	2.22	0.23	1.11
4	0.16	0.86	2.35	0.30	1.24
5	0.16	0.99	2.27	0.38	2.25

The x coordinate is measured in the streamwise direction from the splitter plate tip with the y coordinate normal to x in the transverse direction. For each case, a number of y traverses at fixed x locations were obtained. The two-dimensional data[3–6] at each x location are listed as y (mm), the mean streamwise velocity U (m/s), the streamwise rms fluctuating velocity $\langle u' \rangle$ (m/s), the transverse rms fluctuating velocity $\langle v' \rangle$ (m/s), and the velocity correlation coefficient $\langle u'v' \rangle / (\langle u' \rangle \langle v' \rangle)$, from which the kinematic Reynolds shear stress $\langle u'v' \rangle$ may be obtained.

In making LDV measurements in high-speed flows, there are a number of bias and error sources that must be carefully considered, including velocity bias, fringe bias, velocity gradient bias, particle concentration bias, particle dynamics effects, limitations because of finite counterclockwise resolution, statistical uncertainty because of finite sample size, signal noise, errors because of optical system misalignment, etc. These sources of error and estimates of their magnitudes are discussed in detail in Refs. 4 and 6.

Code Descriptions

NASTAR[7] Navier–Stokes Analysis

Pratt and Whitney's NASTAR code is a viscous-flow analysis that solves the Reynolds-averaged form of the Navier–Stokes equations (RANS) for steady, three-dimensional flows, including the effects of turbulence and heat release caused by chemical reaction. The code was developed at Pratt and Whitney by Rhie and Chow[7] and is based on a significant extension of the pressure-correction methodology used in the TEACH family of codes.[8] The governing equations are approximated using a finite volume method. Rhie and Chow's method provides a single-cell, general curvilinear coordinate procedure that is applicable for Mach numbers ranging from incompressible flow to hypersonic flow. The results described in this study were obtained using the two-equation (k-ε) model for turbulence.[9] Near-wall analysis uses either a wall function or low-Reynolds number wall-integration approach. Compressibility effects can be included using Dash et al.'s[10] form of the Sarkar correction (see Appendix).

For the present calculations, total pressure and temperature profiles were specified at the upstream end of the computational domain. In addition, initial levels of turbulence (k and ε) were specified. A constant value of free static pressure was assumed at the downstream end of the computational domain, which was external to the nozzle.

PAB3D[11,12] Navier–Stokes Analysis

PAB3D (version 13) is a Navier–Stokes analysis developed by NASA LaRC. This code has several computational schemes, different turbulence models, and viscous stress models that can be selected by the user, as described in more detail in Refs. 13–16. The RANS equations are solved by neglecting all streamwise derivatives of the viscous terms. The Roe upwind scheme with first-, second-, or third-order accuracy can be used in evaluating the explicit part of the governing equa-

tions, and the van Leer scheme is used to construct the implicit operator. The diffusion terms are centrally differenced and the inviscid flux terms are upwind differenced. Two finite volume splitting schemes are used to construct the convective flux terms. For jet-mixing computations, the van Albeda solution limiter is required to obtain a smooth converged solution. Other solution limiters available in the code include min–mod, Spekreijse–Venkat (S–V), and a modified S–V.

The standard Jones and Launder[9] linear k-ε turbulence model and three nonlinear algebraic Reynolds stress models (ASM) are implemented in the PAB3D code: Shih–Zhu–Lumley, Gatski–Speziale, and Girimaji. All of these models are robust for general application and are available through user-selectable flags in an auxiliary input file. Implementation of the turbulence model equations are uncoupled from the RANS equations. Furthermore, the turbulence equations are solved with a smaller time step, typically one-half to one-quarter of that is used for the principle flow solution. The final solution is not affected by this time-step difference. However, slower overall solution convergence can result if the time-step ratio is much below one-fourth. Several compressibility correction factors are also available in the code. Models proposed by Wilcox,[17] Sarkar,[18] Ristocelli,[19] and Zeman[20] have been implemented in the PAB3D (version 13) code. The Zeman or Wilcox model uses a Heaviside step function to ensure that the compressibility correction is activated for local flow Mach numbers near or greater than 1.

In the two-equation k-ε turbulence model approach, a near-wall damping function is required at wall boundaries for the ε equation. It is commonly known as the low-Reynolds number formulation. However, the wall function approximation is not used in PAB3D applications.

NPARC[21] Navier–Stokes Analysis

The NPARC code is a Navier–Stokes solver jointly supported by NASA Lewis Research Center and U.S. Air Force Arnold Engineering Development Center through the NPARC Alliance.[21] NPARC was previously known as the PARC code. The basis of the NPARC code are the RANS equations in conservation law form. Steady-state flows are simulated using the pentadiagonal form of the Beam and Warming approximate factorization algorithm. Second-order-accurate central differencing is used for the spatial discretization, which requires artificial dissipation for stability. It may be operated in inviscid or viscous (laminar or turbulent) mode. Generalized boundary conditions allow any portion of the grid to be specified as a boundary, and multiple block interfacing is available to simplify the grid-generation process for complex geometries.

As a result of recent improvements to the code since the establishment of the NPARC Alliance, several one- and two-equation turbulence models are available for use with the NPARC code, with the Chien low Reynolds number k-ε model[22] used for the mixing studies investigated here. The turbulent kinetic energy and dissipation equations are solved uncoupled from the main flow equations using an upwind biased solver. The compressibility correction from Sarkar and Balakrishnan[23] (see the Appendix) is available for use with the Chien model in NPARC. In addition, the axisymmetric dissipation correction of Pope[24] and the two-equation k-ε model of Thies and Tam[25] were incorporated into the code for this study.

GIFS3D[26] Navier–Stokes Analysis

The GIFS code (generalized implicit flow solver) was developed by Boeing Commercial Airplane Company for the U.S. Air Force for use in analyzing rocket plumes. It solves the full Navier–Stokes equations discretized in finite volume form with the MacCormack implicit algorithm. Features of the code include reacting chemistry and particle models, and several grid capabilities including mismatched zones, Chimera, moving, and adaptive grids. In addition, the code contains a two-equation (k-ε) model[27] with an option to include a compressibility correction from Childs and Caruso.[28]

NASTD[29] Navier–Stokes Analysis

NASTD is a general-purpose Euler Corporation and Navier–Stokes solver developed at McDonnell Douglas. NASTD operates in two or three dimensions with structured (patched and overlapping) and unstructured grids. Any valid grid can be utilized, NASTD places no restrictions on the point or slope discontinuities at zone interfaces. A mature zone-coupling technique ensures continuity of the solution across zone boundaries. NASTD has a library of boundary condition routines available on a point-by-point basis.

NASTD has been used for flows from nearly incompressible speeds ($M < 0.05$) to hypersonic speeds. Turbulence can be modeled by a variety of algebraic, one- and two-equation turbulence models. The default scheme for most NASTD applications is the Spalart–Allmaras one-equation model that provides reasonable accuracy for attached and separated boundary layers as well as shear layers. A low Reynolds' number form of the Menter two-equation model is the preferred higher-order model. The Menter model is a hybrid k-ω/k-ε two-equation model (also called an SST model), with k-ω used in near-wall regions and k-ε used away from the wall and in free shear-layer regions.

NASTD incorporates a number of user-selectable (by zone) solution algorithms, with the first-order, approximately factored implicit scheme being used in the following study. The explicit spatial operator is a second-order Roe flux difference split scheme. The standard upwind operator has been replaced by a physical space scheme that retains the upwind-biased scheme stability properties with reduced numerical dissipation. Optionally, the scheme may be switched to various first- through fifth-order schemes, and total variation diminishing (TVD) limiters may be activated. Other available schemes include standard second-order central differencing with added second- and fourth-order dissipation. Ideas motivating the origin of NASTD are described in Bush.[29] More recent algorithm enhancements are described in Cain and Bush.[30]

Discussion of Results

Supersonic Round Jet

The supersonic, Mach 2, round jet case of Seiner et al.[1] was selected as the first benchmark case for calibrating the five Navier–Stokes analyses used by members of the HSCT nozzle team. The "Seiner" nozzle has a jet-exit Mach number typical of the primary flow from the mixer chutes. The Seiner jet exhausts into stationary air. The flow exits the nozzle as a largely inviscid flow with a small wall boundary layer. The boundary layer spreads radially, eventually reaching the centerline axis. The region from the nozzle exit plane to this centerline point is called the potential core.

Three computational grids were generated for this analysis study. A baseline grid of 241 by 121 was generated. The axial/radial extent of the computational domain is $-7.22D$ upstream of the exit plane (plenum), $25D$ downstream, and $11.1D$ away from the centerline. This grid was clustered near the nozzle wall to resolve the shear-layer development. A schematic view of the geometry and the corresponding baseline computational grid is shown in a truncated view in Fig. 1. A second grid (WF) was also generated, removing cells near the wall for evaluating the wall function turbulence model option. The mesh was clustered near the nozzle wall surface, providing a y^+ of 50–100.

Two specific cases were studied by all codes: a cold-flow (T_{tj} = 104°F) operating point and a hot-flow (T_{tj} = 1550°F) operating point. All analyses were performed using the same baseline grid with the basic k-ε turbulence model. No corrections for compressibility or thermal gradient effects (P_{rt} = 0.9) were applied in the baseline analysis run. All codes also mod-

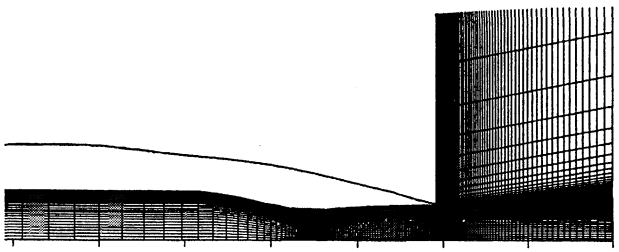

Fig. 1 Baseline grid for Seiner nozzle geometry.

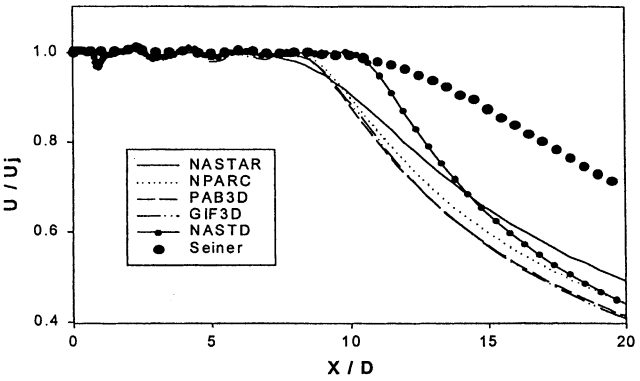

Fig. 2 Centerline axial velocity decay comparisons for Seiner nozzle, T_{tj} = 104°F.

eled the near-wall viscous flow by integrating directly to the wall (except GIF3D).

Results of the baseline analyses are shown in Figs. 2 and 3a–3c. Comparisons for the cold-flow (Fig. 2) and hot-flow (Figs. 3a–3c) cases are presented in terms of centerline distributions of axial velocity (normalized to the jet-exit velocity), Mach number, and total temperature (normalized to the jet upstream total temperature). One can look at these results in basic flow parameters such as the length of the potential core of the rate of mixing in the far field or in terms of integrated parameters such as mixedness or signature (acoustic or infrared). For the present study, agreement in the basic flow parameters of better than 10% will be considered good, whereas agreement of less than 10% is poor. The results indicate that all codes produce essentially the same results, but they do not accurately model the measured data. All analyses break from the potential core sooner than the measured data (mix faster). All of the code results predict a slightly underexpanded jet core with weak Mach waves. The data also show this to a lesser degree. It is interesting to note that the Mach number distribution in Fig. 3b shows NASTD performing better than the other codes (predicting a longer potential core); however, this conclusion cannot be drawn from the velocity and temperature comparisons. To verify the consistency of the calculated results, a grid resolution study was conducted. Finer grid (by a factor of 4) and coarser grid (by a factor of 4) NPARC calculations were performed, with little change noted from the baseline grid results.

Figures 4a–4c illustrate a global overview of the centerline flowfield behavior provided by a range of NASTAR predictions. The experimental data indicate that as the jet total temperature increases, the length of the potential core decreases and the rate of far-field decay also increases. The end of the experimental potential core occurs around x/D = 10, whereas the end of the computational potential core occurs around 7–8. It is also interesting to note that the maximum value of turbulence kinetic energy on the centerline occurs near the end of the potential core, and that the chosen normalization produces a parameter that is largely independent of jet total temperature.

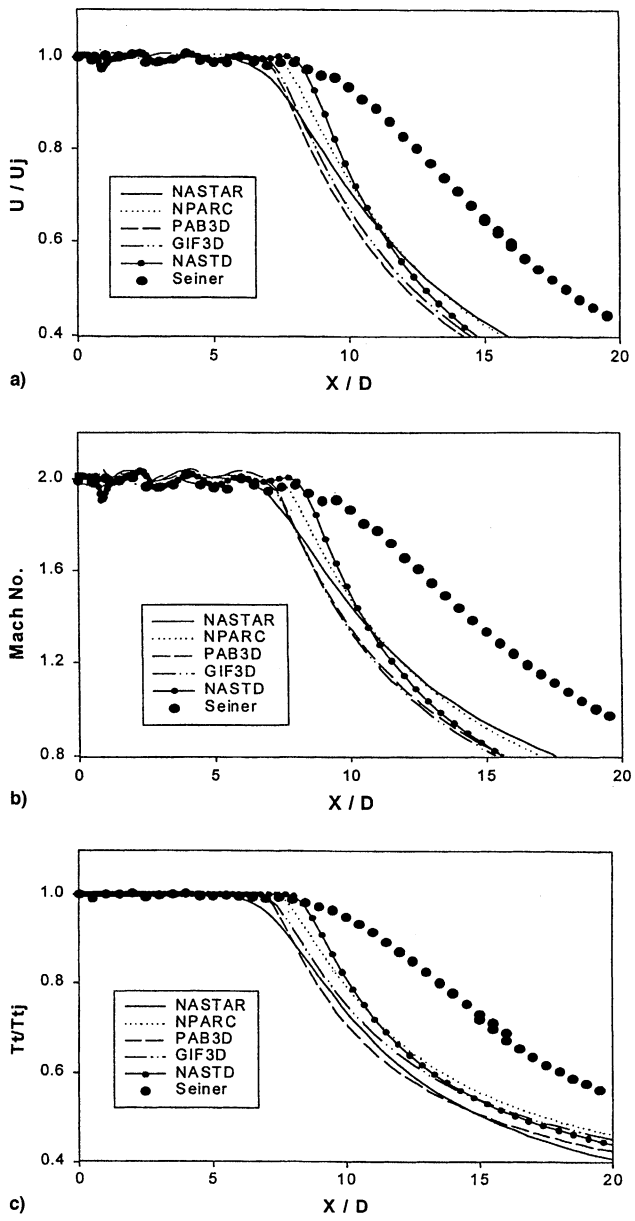

Fig. 3 Centerline a) axial velocity b) Mach number, and c) total temperature decay comparisons for Seiner nozzle, T_{tj} = 1550°F.

Another way to view the results seen in Figs. 4a and 4b is to display the appropriate results in a normalized log–log plot of the centerline velocity vs the axial distance. Downstream of the potential core, an ideal round jet will asymptotically decay as $1/x$. Figure 4c displays the cold-flow results for all codes in such a format. The NASTAR results and the Seiner et al.'s[1] experimental data are displayed for both the cold- and hot-flow cases. All of the codes predict a jet decay rate (for hot and cold cases), close to the classical $1/x$ round jet decay rate (Table 3). The Seiner cold-flow case decay rate is less than two-thirds the expected value.

In addition to the preceding baseline studies, parametric analyses on the effects of grid density, boundary conditions, and turbulence modeling were performed. Initial NASTAR studies focused on the impact of modeling a static jet with a finite but small coflow (M_∞ from 0.05 to 0.10) and the effect of plenum turbulence level (I = turbulence intensity, 1–10%). Figure 5 illustrates that the jet decay characteristics are largely independent of both. Figure 5a also displays the effect of approximating the nozzle near-wall boundary layer with wall functions. This approximation is frequently used in large complex three-dimensional problems as an effective way to control

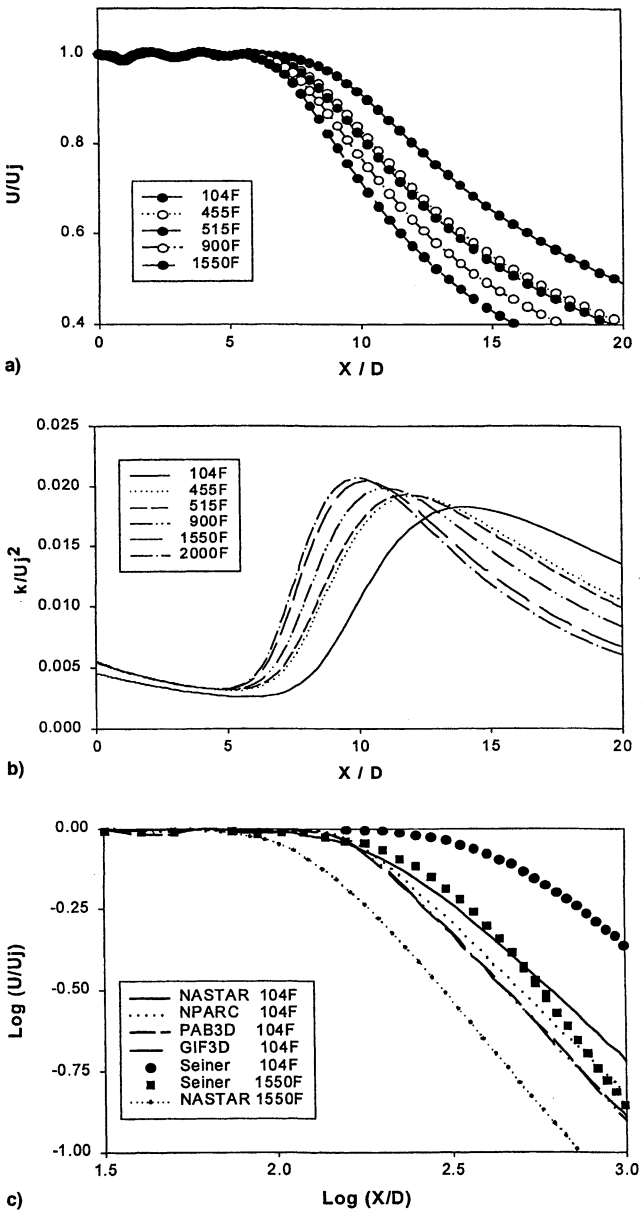

Fig. 4 a) NASTAR predictions of centerline velocity decay over range of T_{tj} conditions, b) NASTAR predictions of normalized turbulence energy over range of T_{tj} conditions, and c) comparison of centerline velocity decay characteristics for T_{tj} = 104 and 1550°F.

the number of grid points used in a simulation. The results shown in Fig. 5a, using the baseline grid, indicate that both wall integration and wall function produce approximately the same potential core length; however, the predicted far-field decay using wall functions is substantially in error from the measured data. A closer look at both solutions inside the nozzle verifies that they are indeed substantially the same. The observed difference in the external flow development has been traced to grid resolution of the jet shear layer. A new calculation was executed using a wall function grid for the internal flow and a grid more consistent with the wall integration approach for the external flow, e.g., 5 to 6 radial grid points were added between the inner- and outer-flow y^+ lines. Figure 5b verifies that grid resolution in the shear was the primary cause of the errors observed in Fig. 5a.

Parametrics have also been performed on the effect of turbulence modeling corrections to the basic k-ε turbulence model on the predicted jet flowfield. For high-speed jet flows, corrections to the baseline k-ε model for compressibility[29] and vortex stretching[22] have been proposed (see Appendix). Figure

Table 3 Velocity decay rate

Code	T_{tj} = 104°F	T_{tj} = 1550°F
NASTAR	0.98	1.33
NPARC	1.06	——
PAB3D	1.12	——
GIF3D	1.16	——
Seiner	0.63	1.51

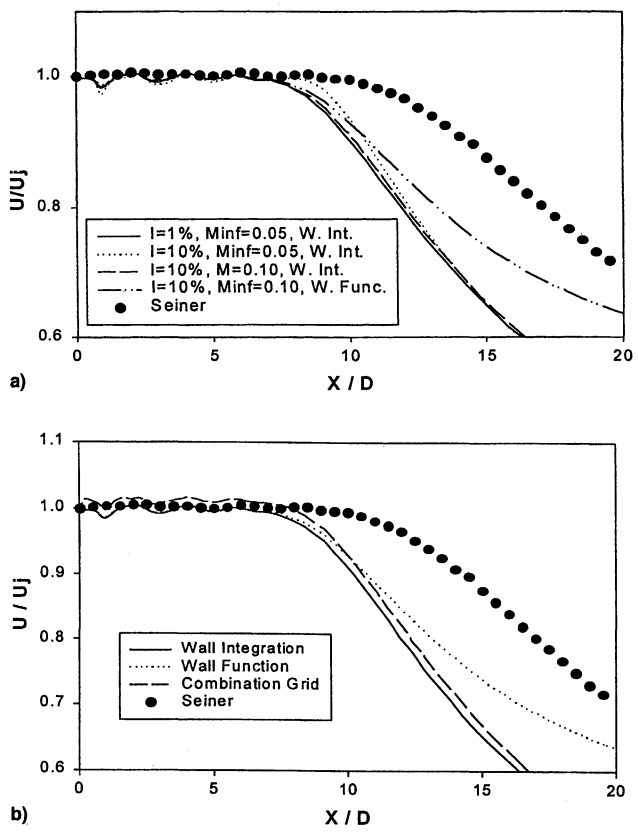

Fig. 5 Effect of a) boundary condition and b) wall grid modeling on NASTAR predictions, Seiner nozzle T_{tj} = 104°F.

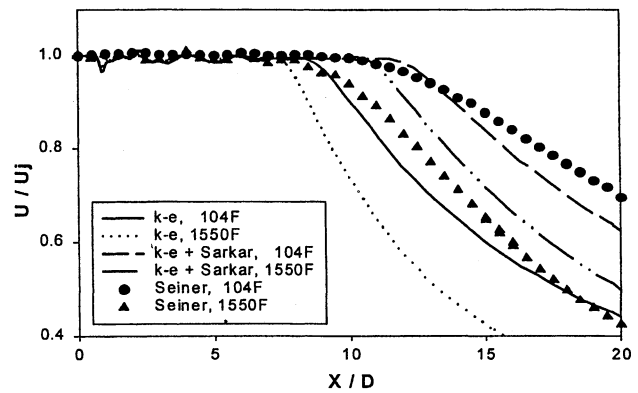

Fig. 6 Effect of compressibility corrections on centerline velocity decay in NPARC, Seiner nozzle.

6 illustrates the effect of the Sarkar[18] corrections on both the cold and hot Seiner jet flows. In each case, the Sarkar correction slows the jet shear-layer spread rate, extending the length of the potential core, and bringing the predictions closer to the experimental data. The calculated shear-layer spread rate illustrates this more clearly (Fig. 7). In each calculation, the jet spreads at two distinct rates, an initial rate in the potential core, and a faster rate downstream of the transition region ($x/D \approx$ 10). The effect produced by the Sarkar correction shows rel-

ative agreement with the LaRC curve; however, the LaRC curve predicts a larger reduction in spread rate. No experimental data are shown because radial profiles for these cases have not been released at present.

Figure 8 presents NPARC centerline velocity distribution for the baseline or standard k-ε model as well as for the calculations including the effects of the Sarkar and Pope[22] corrections, individually and combined, for only the cold-flow case. Each correction individually improves the NPARC predictions; however, when combined, the results are not good. From this log–log plot, one can see that these models affect only the shear-layer growth effect on the potential core and not the far-field decay rate.

Additional turbulence modeling parametrics were performed using PAB3D. The results shown in Figs. 9a and 9b illustrate the effect of six turbulence model variations (Table 4), performed by General Electric Aircraft Engine Co. for the Seiner et al.[1] cold-flow (104°F) and hot-flow (1550°F) cases, using the PAB3D code. The basic equations for the k-ε model, its corrections, and the appropriate constant used, are defined in the Appendix. While the Zeman[18] compressibility correction (run 4) apparently gives the best agreement with experimental data for the cold-flow case, it significantly overshoots the data (run 10) in the hot-flow case. As expected, the compressibility correction decreases the predicted baseline mixing rate, but by a larger rate than observed in the data. The Zeman correction,[20] as implemented in PAB3D, is larger than the Sarkar and Balakrishnan[23] correction in NPARC.

Calculations were also performed using the Thies and Tam[25] set of constant turbulence coefficients parameters proposed for the k-ε turbulence model (see Appendix). Thies and Tam performed calculations for the Seiner et al. nozzle geometry by initializing their calculations from the nozzle exit plane using an assumed top-hat velocity profile, in contrast to the procedure used earlier, starting upstream in the nozzle plenum region, allowing the boundary layer to develop. The NPARC calculations, shown in Figs. 10 and 11, compare the cold- and hot-flow results obtained using the Thies and Tam coefficients. While the Thies and Tam results are better than the baseline results, they are not as good as the results originally reported.

Finally, attempts were made to account for thermal gradient effects on the jet mixing rate by decreasing P_{rt} from the normal value used (0.9) to 0.5. The effect is negligible for the velocity field but it is more noticeable for the total temperature, this is best seen in terms of the log–log behavior shown in Fig. 12. The predicted trend is in the correct direction, i.e., heated jets mix faster than isothermal jets. The effect on core length is less than 2%, whereas the far-field decay rate increases by about 6%.

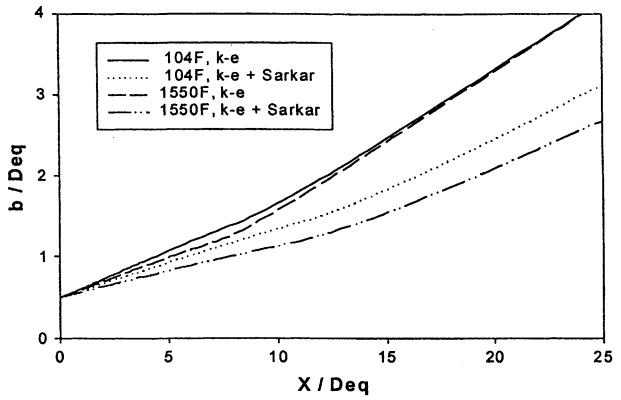

Fig. 7 Effect of compressibility corrections on shear-layer spread rate in NPARC, Seiner nozzle.

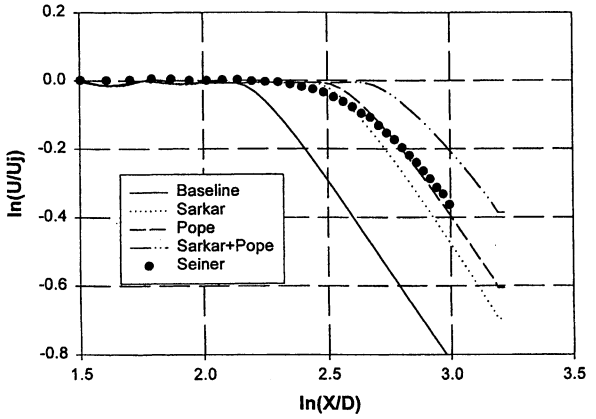

Fig. 8 Effect of k-ε turbulence model corrections in NPARC, Seiner nozzle T_{ij} = 104°F.

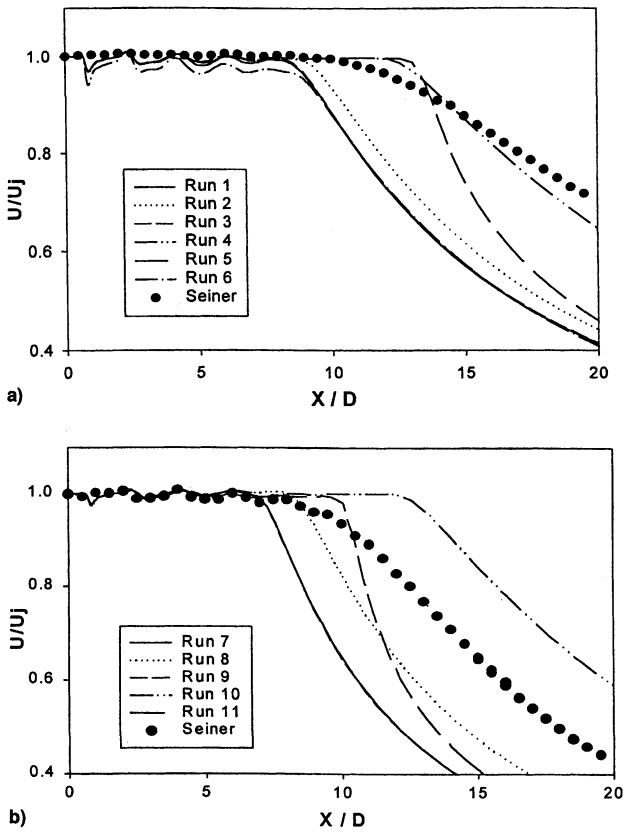

Fig. 9 Effect of turbulence modeling on PAB3D predictions, Seiner nozzle T_{ij} = a) 104 and b) 1550°F.

Table 4 PAB3D turbulence model parametrics

PAB3D run	Turbulence model
1,7	Jones and Launder k-ε
2,8	Jones and Launder k-ε, Zeman compressibility
3,9	Jones and Launder k-ε, high Re form in plume
4,10	Jones and Launder k-ε, high Re form in plume, Zeman compressibility
5,11	Wilcox k-ω
6	Shih and Lumley nonlinear ARS

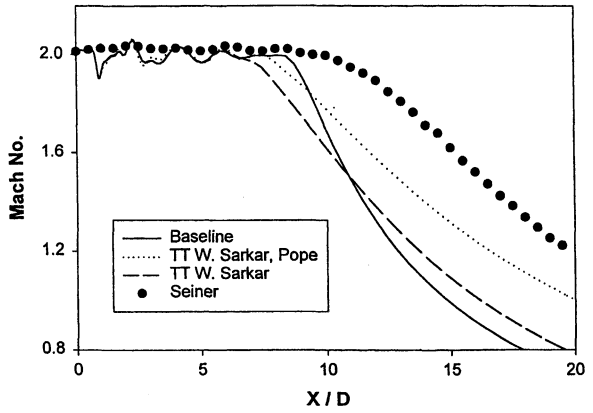

Fig. 10 Effect of Thies and Tam's[25] turbulence model on NPARC centerline Mach number predictions, Seiner nozzle T_{tj} = 104°F.

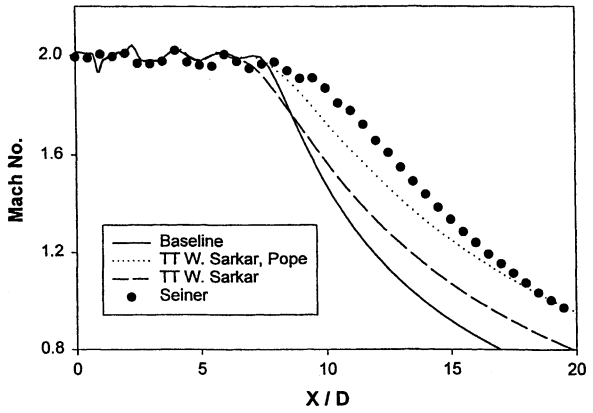

Fig. 11 Effect of Thies and Tam's[25] turbulence model on NPARC centerline Mach number predictions, Seiner nozzle T_{tj} = 1550°F.

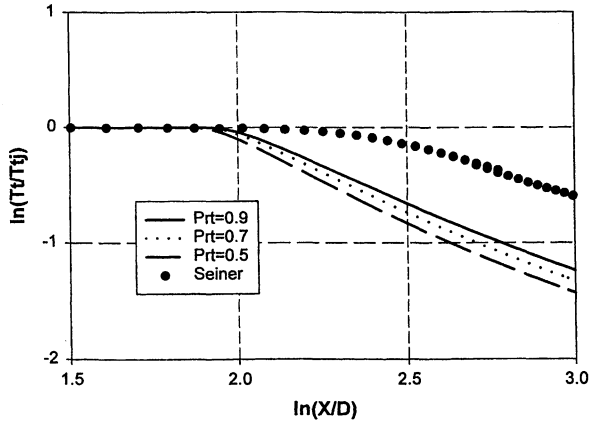

Fig. 12 Effect of turbulent Prandtl number on jet mixing.

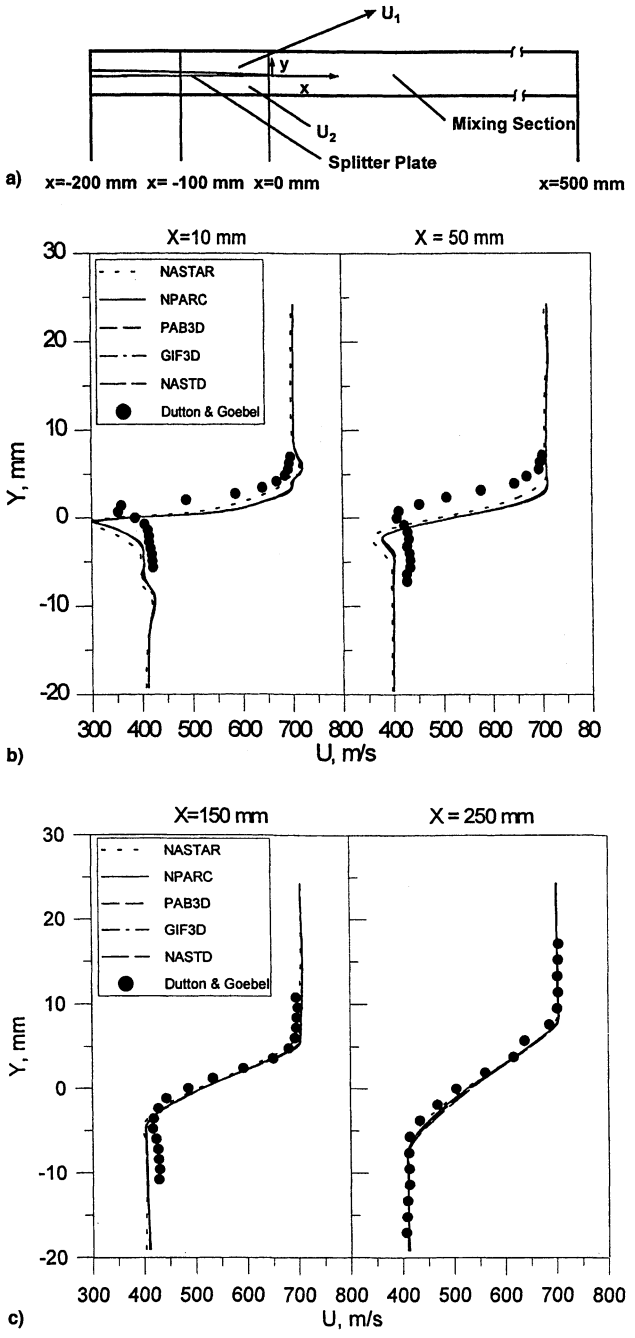

Fig. 13 a) Schematic of Dutton and Goebel plane shear-layer geometry; b) velocity profile comparisons for Dutton and Goebel case 2, baseline k-ε model; and c) velocity profile comparisons for Dutton and Goebel case 2, baseline k-ε model.

Dutton-Goebel Planar Shear Layer

The two-dimensional supersonic layer of Goebel and Dutton was the second flow case investigated by the five members of the HSCT nozzle team. The experimental configuration, as discussed earlier, had two streams separated by a splitter plate upstream of the mixing section. From the choice of several different cases, case 2 was calculated by all five members of the team. The two streams in case 2 had Mach numbers of 1.91 and 1.36 and total temperatures of 1041 and 71.6°F, respectively. A previous study[31] examined the effect of grid resolution and inflow boundary conditions on mixing-layer predictions. Based on the results of this study, a mesh with 281 points in the streamwise direction (91 upstream of the splitter plate trailing edge and 190 downstream), and 131 points in the vertical direction, was used as the baseline computational grid.

A view of the computational domain is shown in Fig. 13. The grid for the following calculations was packed close to the splitter plate wall for use with wall-integration turbulence models.

All of the calculations were 200 mm (7.87 in.) upstream of the splitter plate trailing edge to allow the boundary layer and momentum thicknesses generated by the computations to closely match those measured in the experiment at the trailing edge of the splitter plate. The exit of the computational region ended at 500 mm (19.86 in.) downstream of the trailing edge, and the height of the mixing section was 48 mm (1.89 in.). In the experiment, the top and bottom walls were diverged slightly to account for the blockage effect of wall boundary-layer growth.

Calculations were obtained for all codes using fixed boundary conditions for the two supersonic inflows. Figures 13b and

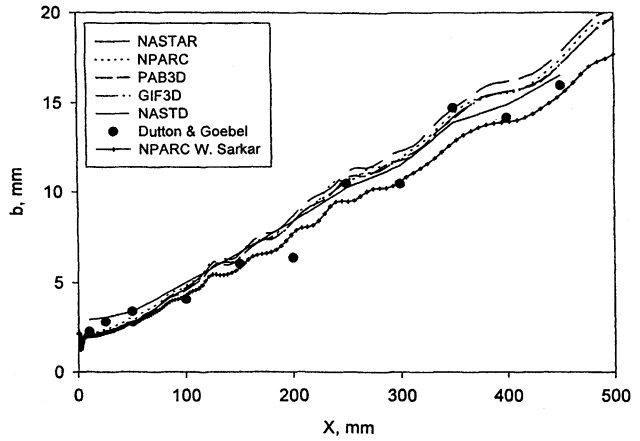

Fig. 14 Comparison of shear-layer spreading for Dutton and Goebel case 2 flow.

13c show the velocity profiles of the five computations with LDV measurements at several locations in the mixing region. Except for very near the splitter plate exit plane, all of the codes produce nearly the same results throughout the mixing region. The NASTAR results (using a wall-function turbulence model) deviate from the other solutions until 100 mm downstream of the splitter plate trailing edge. In comparing the solutions to the experimental data, the computations are not in good agreement with the data in the wake region near the splitter plate trailing edge, but do match the experimental data farther downstream in the mixing region.

Figure 14 shows the mixing layer growth, (b), which is defined as the distance from the location where the axial velocity is greater than U_2 by 12% of ($U_1 - U_2$), to the location where the axial velocity is less than U_1 by 12% of ($U_1 - U_2$). The computed results are in good overall agreement with the experimental data.

The effect of compressibility correction on the results was further examined with the NPARC code. An examination of the velocity profiles for the NPARC solutions obtained with and without the Sarkar[18] correction to the kinetic energy production do not demonstrate a significant difference between the two computed results. This is most likely because the convective Mach number was relatively low, 0.46, for this flow with two supersonic streams. The comparison of mixing-layer thicknesses in Fig. 14 shows somewhat decreased mixing for the NPARC calculation obtained with the Sarkar[18] correction.

Case 4 was also briefly examined as a more interesting case with strong compressibility effects. For this case the Mach numbers of the two streams were 2.35 and 0.30, and the total temperatures were 188.6 and 62.6°F, respectively, yielding a convective Mach number of 0.86. Unlike case 2, with fixed boundary conditions specified for the two inflows, the subsonic inflow for this case was set to a free boundary with total pressure and total temperature specified, and the static pressure measured at the exit plane in the experiment was set as the computational exit station boundary. Initial calculations with the NPARC code used slip walls for the top and bottom walls, as done for case 2. The core flow Mach number of the subsonic stream, however, was observed to accelerate significantly through the duct, unlike that documented from the experiment, where the core flow of the subsonic stream remained near Mach 0.3. To more accurately simulate the conditions of the two core flows in the experiment, a number of simulation modifications were tried and yielded positive agreement with data. However, because these calculations were somewhat arbitrary, no results for this case are included in the text.

Concluding Remarks

Five organizations participated in a code-evaluation effort to determine the applicability of each team member's Navier–Stokes code to model the phenomena in the HSCT exhaust nozzle. The effort considered several model problems, chosen to examine representative mixing phenomena encountered in a mixer–ejector nozzle. The configurations selected were Seiner's supersonic heated round nozzle and Goebel and Dutton's planar shear layer.

Comparisons of the numerical results obtained from the five different codes demonstrated that all codes produced similar results when using common grids, boundary conditions, and turbulence models. Comparisons with experimental data, however, produced mixed results, i.e., good agreement for the mixing of planar shear layers, but poor agreement for the mixing of round jets.

While the numerical simulations obtained showed little sensitivity to some boundary conditions, typically not known a priori or measured, e.g., upstream turbulence level, they showed strong dependence on the choice of turbulence model. In addition, it was also noted that the choice of near-wall treatment was important in accelerating flows.

Finally, the results obtained confirmed that a multicompany effort can jointly contribute to a nozzle design analysis effort, when a common modeling approach is established. Based on the computational results obtained to date, one can recommend the following procedures for modeling shear-layer mixing problems reliably and consistently across codes:

1) Use basic k-ε or an equivalent two-equation turbulence model with no corrections for operating conditions, i.e., compressibility, thermal effects, etc.

2) Assume the turbulent Prandtl number (P_{rt}) is 0.9.

3) Model static flow conditions by assuming a small forward-flight component ($M_\infty = 0.05$) to ensure computational stability.

4) Use wall integration rather than wall function where possible.

Appendix: k-ε Turbulence Model and Corrections

A standard form for the k-ε two-equation turbulence model is given next. While not all codes have implemented this exact form and all codes have different near-wall low Reynolds number models, the turbulence coefficients refer to the same terms in each case:

$$\rho \frac{dk}{dt} = \frac{\partial}{\partial x_i}\left[\left(\frac{\mu_T}{\sigma_k}\right)\frac{\partial k}{\partial x_i}\right] - \rho\varepsilon + \rho P$$

$$\rho \frac{d\varepsilon_s}{dt} = \frac{\partial}{\partial x_i}\left[\left(\frac{\varepsilon_s + \varepsilon_c}{\varepsilon_s}\right)\left(\frac{\mu_T}{\sigma_s}\right)\frac{\partial \varepsilon_s}{\partial x_i}\right] + \frac{\varepsilon_s}{k}[C_{\varepsilon 1}P - \rho\varepsilon_s(C_{\varepsilon 2} - C_3\chi)]$$

$$\mu_T = C_\mu \rho[k^2/(\varepsilon_s + \varepsilon_c)] = \text{turbulent viscosity}$$

$$\varepsilon = \varepsilon_s + \varepsilon_c = \text{turbulence dissipation}$$

$$\bar{M}_T = \sqrt{2k/a} = \text{turbulence Mach number}$$

$$\varepsilon_c = C\varepsilon_s(\alpha_1 \bar{M}_T^2 + \beta \bar{M}_T^4)$$

$$\bar{M}_T = M_T - \lambda$$

where χ is Pope's[24] vortex stretching parameter, P is the turbulent kinetic energy production term, λ is Zeman's[20] Heaviside lag function, and σ_k and σ_ε are the turbulence Prandtl numbers. The subscript s refers to the solenoidal or incompressible contribution, and c refers to the compressible contribution. The preceding form of the k-ε equations is from Dash.[10] For many others, the only correction for compressibility effects (ε_c) is through a quadratic M_T term ($\beta = 0$), which is included only in the source term of the k equation. A standard set of coefficients for this model is provided in Table A1. In addition, Dash[10] suggests using $\beta = 60$ for the quartic correction term and $\lambda = 0.1$ for the lag term.

Table A1 Two-equation turbulence model coefficients

Model	C_μ	$C_{\varepsilon 1}$	$C_{\varepsilon 2}$	$C_{\varepsilon 3}$, Pope[24]	Pr_T	σ_k	σ_ε	α_1, Sarkar[18]
Jones and Launder[9]	0.09	1.44	1.92	0.79	1.00	1.00	1.30	0.3–1.0
Thies and Tam[25]	0.0874	1.40	2.02	0.822	0.422	0.324	0.377	0.518
Chien[22]	0.09	1.35	1.80	0.79	0.90	1.00	1.30	1.0

Thies and Tam[25] proposed that the standard coefficients for the k-ε turbulence model, even with Sarkar[18] and Pope[24] corrections for compressibility and centerline vortex stretching, do not represent any broad range of physical applicability, rather that they were developed largely for boundary layer and low Mach number plane mixing-layer data. Thies and Tam instead offered a new set of empirical coefficients (shown in Table A1) obtained from an optimization of calculations performed over a range of subsonic to supersonic jet flows.

Acknowledgments

This work was supported by a Task Order contract from the NASA Lewis Research Center. The authors would like to thank K. Early, General Electric Aircraft Engine Co.; R. Henke and A. Guthrie, Boeing Commercial Airplane Co.; A. Cain and T. Austin, McDonnell Douglas Corporation; and J. Seiner and P. Pao, NASA Langley Research Center, for their assistance in obtaining the experimental data and performing the calculations using their organizations respective analyses.

References

[1]Seiner, J. M., Ponton, M. K., Jansen, B. J., and Lagen, N. T., "The Effects of Temperature on Supersonic Jet Noise Emission," AIAA Paper 92-02-046, May 1992.

[2]Kline, S. J., Cantwell, B. J., and Lilley, G. M., *1980–1981, AFOSR-HTTM-Stanford Conference*, Vol. 1, Stanford Univ. Press, Stanford, CA, 1982, p. 368.

[3]Goebel, S. G., "LDV Measurements of a Supersonic Mixing Layer," M.S. Thesis, Dept. of Mechanical and Industrial Engineering, Univ. of Illinois at Urbana–Champaign, IL, May 1988.

[4]Goebel, S. G., Dutton, J. C., Krier, H., and Renie, J. P., "Mean and Turbulent Velocity Measurements of Supersonic Mixing Layers," *Experiments in Fluids*, Vol. 8, No. 5, 1990, pp. 263–272.

[5]Goebel, S. G., "An Experimental Investigation of Compressible, Turbulent Mixing Layers," Ph.D. Dissertation, Dept. of Mechanical and Industrial Engineering, Univ. of Illinois at Urbana–Champaign, IL, May 1990.

[6]Goebel, S. G., and Dutton, J. C., "An Experimental Study of Compressible, Turbulent Mixing Layers," *AIAA Journal*, Vol. 29, No. 4, 1991, pp. 538–546.

[7]Rhie, C. M., and Chow, W. L., "Numerical Study of the Turbulent Flow Past and Airfoil with Trailing Edge Separation," *AIAA Journal*, Vol. 21, No. 11, 1983, pp. 1525–1532.

[8]Patankar, S. V., *Numerical Heat Transfer and Fluid Flow*, Hemisphere, New York, 1980.

[9]Jones, W. P., and Launder, B. E., "The Prediction of Laminarization with a Two-Equation Model of Turbulence," *International Journal of Heat and Mass Transfer*, Vol. 15, No. 2, 1972, pp. 301–331.

[10]Dash, S. M., Kenzakowski, D. C., Sinha, N., and Hosangadi, A., "Simulation of High-Speed Jets: Turbulence and Two-Phase Flow Modeling," AIAA Paper 92-3440, July 1992.

[11]Abdol-Hamid, K. S., Uenishi, K., and Turner, W., "Three-Dimensional Upwinding Navier-Stokes Code for k-ε Model for Supersonic Flows," AIAA Paper 91-1669, 1991.

[12]Abdol-Hamid, K. S., Lakshmanan, B., and Carlson, J. R., "Application of Navier-Stokes Code PAB3D with k-ε Turbulence Model to Attached and Separated Flows," NASA TP-3480, Jan. 1995.

[13]Abdol-Hamid, K. S., Carlson, J. R., and Lakshmanan, B., "Application of Navier-Stokes Code PAB3D to Attached and Separated Flows for Use with k-ε Turbulence Model," NASA TP-3489, Aug. 1994.

[14]Abdol-Hamid, K. S., "A Multiblock/Multizone Code (PAB3D-v2) for the Three-Dimensional Navier-Stokes Equations: Preliminary Applications," NASA CR-182032, Oct. 1990.

[15]Abdol-Hamid, K. S., Carlson, J. R., and Pao, S. P., "Calculation of Turbulent Flows Using Mesh Sequencing and Conservative Patch Algorithm," AIAA Paper 95-2336, July 1995.

[16]Abdol-Hamid, K. S., "Implementation of Algebraic Stress Model in a General 3-D Navier-Stokes Method (PAB3D)," NASA CR-4702, Dec. 1995.

[17]Wilcox, D. C., "Progress in Hypersonic Turbulence Modeling," AIAA Paper 91-1785, June 1991.

[18]Sarkar, S., "Modeling the Pressure-Dilatation Correlation," NASA CR 187566, Inst. for Computer Applications in Science and Engineering, Rept. 91-42, May 1991.

[19]Ristocelli, J. R., "A Representation for the Turbulent Mass Flux Contribution to Reynolds-Stress and Two-Equation Closures for Compressible Turbulence," Inst. for Computer Applications in Science Engineering, Rept. 93-88, Nov. 1993.

[20]Zeman, O., "Dilatational Dissipation: The Concept and Application in Modeling Compressible Mixing Layers," *Physics of Fluids*, Vol. XX, No. 2, May 1990.

[21]Cooper, K., "NPARC 2.0-Features and Capabilities," AIAA Paper 95-2609, July 1995.

[22]Chien, K.-Y., "Predictions of Channel and Boundary Layer Flows with a Low-Reynolds-Number Turbulence Model," *AIAA Journal*, Vol. 20, No. 1, 1982, pp. 33–38.

[23]Sarkar, S., and Balakrishnan, L., "Application of a Reynolds Stress Turbulence Model to the Compressible Shear Layer," NASA CR 182002, Inst. for Computer Applications in Science and Engineering, Rept. 90-18, Feb. 1990.

[24]Pope, S. B., "An Explanation of the Turbulent Round-Jet/Plane Jet Anomaly," *AIAA Journal*, Vol. 16, No. 3, 1978, pp. 279–281.

[25]Thies, A. T., and Tam, C. K. W., "Computation of Turbulent Axisymmetric and Nonaxisymmetric Jet Flows Using the k-ε Model," *AIAA Journal*, Vol. 34, No. 2, 1996, p. 309; also 1st Joint CAES/AIAA Aeroacoustics Conf. (AIAA 16th Aeroacoustics Conference), Munich, Germany, June 1995.

[26]Hoffman, J. J., Holcomb, J. E., and Warfield, M. J., "Boeing A882 Navier-Stokes Code," U.S. Air Force Astronautics Lab., Rept. F04611-86-C-0087, July 1994.

[27]Warfield, M. J., "Calculation of Supersonic Interacting Jet Flows," AIAA Paper 89-0666, Jan. 1989.

[28]Childs, R. E., and Caruso, S. C., "On the Accuracy of Turbulent Base Flow Predictions," AIAA Paper 87-1439, June 1987.

[29]Bush, R. H., "External Compressor Inlet Predictions Using an Implicit Upwind, Multiple Zone Approach," AIAA Paper 85-1521, July 1985.

[30]Cain, A. B., and Bush, R. H., "Numerical Wave Propagation Analysis for Stretched Grids," AIAA Paper 94-0172, Jan. 1994.

[31]Georgiadis, N. J., Dudek, J. C., and Tierney, T. P., "Grid Resolution and Turbulent Inflow Boundary Condition Recommendations for NPARC Calculations," AIAA Paper 95-2613, July 1995.